Pergamon

Cement and Concrete Research 31 (2001) 577–588

CEMENT AND CONCRETE RESEARCH

Chloride ion binding capacity of aluminoferrites

Jolán Csizmadia[a], György Balázs[a,*], Ferenc D. Tamás[b,1]

[a]*Department of Building Materials and Engineering Geology, Technical University of Budapest, Budapest, Hungary*
[b]*Department of Silicate and Materials Engineering, University of Veszprém, POB 158, H-8201, Veszprém, Hungary*

Received 3 March 2000; accepted 21 December 2000

Abstract

The hydration of aluminoferrites (C_4AF, C_6AF_2 and C_6A_2F) and their mixture with gypsum (up to 10/5 ratio) was investigated as well as their chloride binding capacity (after immersion in 10% NaCl solution) by thermal tests (DTG and TGA) and X-ray diffraction (XRD). Hydration products of these aluminoferrites are similar to that of C_3A, but amorphous AH_3 and/or FH_3 are formed, and transformation of metastable (hexagonal hydrates) to the stable (hydrogarnet) phase is slower. Iron content of aluminoferrites determines the rate of hydration reactions: hydration rate increases in the order $C_6A_2F > C_4AF > C_6AF_2$. In the case of C_4AF + gypsum mixtures, monosulfate was found prior to the total exhaustion of gypsum. After salt treatment, iron-containing Friedel's salt or Kuzel's salt was found. Characteristics of DTG peaks are described and interpreted. © 2001 Elsevier Science Ltd. All rights reserved.

Keywords: Calcium aluminoferrite; Chloride; Thermal analysis; X-ray diffraction

1. Introduction

The paper deals with the chloride binding capacity of calcium aluminoferrites, especially in the presence of gypsum, a constant ingredient of Portland cement. Former research shows that aluminoferrites react with chloride only after the exhaustion of available sulfates to give a complex aluminoferrite sulfate hydrate (AFm or AFt),[2] if the chloride compound is added jointly with mixing water. From this a question arises: Can the anion of the AFm or AFt in hardened cement paste be exchanged by chloride during deicing salt treatment? This is the more important, as high-iron cements are frequently used because of their high sulfate and seawater resistance.

Hydration products of aluminoferrite phases are similar to those of tricalcium aluminate: In the presence of gypsum, AFm and/or AFt phases (''monosulfate'' and ettringite, respectively) are formed, with the difference that in tricalcium aluminate the calcium to sesquioxide ratio is 3, while in the aluminoferrites this ratio is 2; this means that besides AFm and AFt, aluminum and/or iron hydroxides are formed, too. As most of these hydroxides are amorphous, X-ray diffraction (XRD) cannot be used for identification; alternative methods, e.g., Mössbauer spectroscopy, must be used instead. Reaction rates are, however, different: hydration of aluminoferrites is slower, and this rate is further decreased by the presence of calcium hydroxide, gypsum or both. The first hydration product is ettringite, but this is later transformed to monosulfate, after the exhaustion of available gypsum [1,2].

Several mechanisms exist of chloride binding during cement hydration: chloride may be bonded in the C-S-H gel, as a complex calcium oxychloride, Friedel's salt (a chloride-containing AFm phase, $C_3A{\cdot}CaCl_2{\cdot}H_{10}$), or its high-iron analogue, $C_3F{\cdot}CaCl_2{\cdot}H_{10}$ may form too, especially at low temperatures. In sulfate-resistant Portland cement, if a high amount of aluminum is bonded as calcium aluminoferrite, rather than tricalcium aluminate, the main product is this latter analogue, even at room temperature [3].

Friedel's salt is stable in basic solutions (pH >12), but is destabilised at lower pH values (e.g., by carbonation). If carbonation degree is low, other phases of hydrated cement (e.g., lime hydrate or C-S-H) gel buffer pH value, Friedel's

* Corresponding author. Tel.: +36-1-463-2226; fax: +36-1-463-3450.
E-mail address: balazs@vasbeton.vbt.bme.hu (G. Balázs),
[1] Tel.: +36-88-423-091; fax: +36-88-423-091.
E-mail address: tam043@almos.vein.hu (F.D. Tamás).

[2] Conventional cement chemical nomenclature is used in most cases. The following symbols are used: C = CaO, S = SiO_2, A = Al_2O_3, F = Fe_2O_3, H = H_2O, $\hat{S}$ = SO_3, $\hat{C}$ = CO_2. AFm and AFt mean calcium aluminoferrite monosubstituted, and calcium aluminoferrite, trisubstituted, respectively.

PII: S0008-8846(01)00458-6

salt, and possibly other AFm phases locally survive [4]. Other factors cause a decrease of pH as the presence of acid additives or aggregates (silica fume and similar) affect the stability of Friedel's salt and, as a consequence, the resistance of cement against deicing salt treatment.

The stability of Friedel's salt in concrete structural elements is somewhat more complicated. When concrete slabs are subjected to atmospheric carbonation and chloride attack simultaneously, then the surface carbonation (in the top 5 mm layer) is so severe, that not only Friedel's salt, but also ettringite do not exist any more [5].

Chloride binding of cement is influenced by other factors, too, e.g., alkali content appears to have an inhibiting effect on the chloride binding capacity. This fact, however, is overshadowed by a conjoint strong elevation of the OH^- ion concentration in the pore solution, causing a net lowering of the Cl^-/OH^- ratio, which in turn reduces corrosion risk. According to Ref. [6], a threshold chloride content exists for each cement, depending on the alkali, C_3A and aluminoferrite content (of the cement). The cation of the chloride plays a role too: $CaCl_2$ is more dangerous from this point than NaCl. Although more chloride is bound in the former case, this is counteracted by a decreased OH^- concentration.

Further influences on chloride binding should be also taken into consideration, e.g., the sulfate content [7]. A competition occurs between sulfates and chlorides to react with C_3A (or aluminoferrite phases), and this is won by the sulfates, with a simultaneous increase of the Cl^- concentration in the pore solution. The cation of the sulfate plays a role too: the chloride binding capacity of cement decreases rapidly with increasing sulfate contents derived from sodium sulfate and calcium sulfate; at the same sulfate content, however, cement pastes containing $CaSO_4$ have a higher chloride binding capacity than those containing Na_2SO_4 [8].

2. Experimental

2.1. Raw materials, sample preparation and exposure

Three sets of aluminoferrites (corresponding to C_4AF, C_6AF_2 and C_6A_2F) were prepared from calcium carbonate, alumina and iron(III)-oxide powders by pressing them into small cylinders and subjecting them to multiple firing (after regrinding) in an electric furnace in oxidizing atmosphere. Purity and stoichiometry of the aluminoferrites was controlled by XRD, using the data of Tabikh and Weht [9] as well as of Tamás and Kovács [10]. Gypsum was pure natural gypsum rock, the same as used in cement factories. Three series of samples (13 samples in each series) were prepared. Table 1 shows sample and exposure variables.

Aluminoferrite materials were finely ground to pass sieve 0.063 mm, mixed according to Table 1. Water was added to have a similar workability, and the materials were cast into $10 \times 10 \times 50$ mm prisms. After 24 h, prisms were removed, and kept at room temperature (22 ± 3°C), 100% r.h. Steam-curing was done for 6 h, 70°C, followed by a similar treatment as nonsteamed ones. Salt treatment means to keep samples in 10% NaCl solution, between the 28th and 56th days (24 h in the salt solution, followed by 24 h of drying); after this time salt-treated samples were kept at room temperature, 100% r.h.

Table 1
Samples and their exposure

Mass ratio of ferrite (C_4AF, C_6A_2F or C_6AF_2) to gypsum	Curing + exposure
10/0	100% r.h.
10/1	100% r.h.
10/2	100% r.h.
10/3	100% r.h.
10/4	100% r.h.
10/5	100% r.h.
10/1	100% r.h. + salt-curing
10/2	100% r.h. + salt-curing
10/3	100% r.h. + salt-curing
10/4	100% r.h. + salt-curing
10/5	100% r.h. + salt-curing
10/3	Steam-curing + 100% r.h.
10/3	Steam-curing + salt-curing

Examination of hardened samples was done after 24 h, 28, 56, 90 and 180 days.

2.2. Methods of investigation

The main methods of investigation (all samples, at all ages) were thermal tests (TGA/DTG/DTA) using the Derivatograph 1500-Q. In most cases, the DTG curve proved to be adequate, as all peaks are endothermal, thus DTA did not give surplus information as contrasted to the more sensitive DTG curve. Data of thermal tests: inert material — alumina, heating rate — 10°C/min, up to 980°C, in air atmosphere. Evaluation was computer-controlled. The tables give weight losses (in percent of the original weight of the sample). As a secondary method, XRD was used, with CuK_α radiation.

Lack of space does not permit us to present all data. The majority of DTG curves are described qualitatively only, although sample DTG curves or XRD patterns are shown. Details can be retrieved via the corresponding author. Tables 2, 4 and 5) show quantitative results, as calculated (with DTG aid) by the TGA curve, giving gross mass losses between 20°C and 900°C, but subdivided into temperature intervals: 20–130°C, 130–600°C and 600–900°C, corresponding to losses caused by moisture, structural H_2O and CO_2 and/or NaCl, respectively.

2.3. Hydration of C_4AF

Quantitative data (mass losses, by TGA) are presented in Table 2.

Table 2
C_4AF mass losses by TGA (initial sample mass = 100)

Age	24 h				28 days				56 days					90 days					180 days				
Temperature interval	130–600 °C	20–130 °C	600–900 °C	20–900 °C	130–600 °C	20–130 °C	600–900 °C	20–900 °C	130–600 °C	20–130 °C	600–900 °C		20–900 °C	130–600 °C	20–130 °C	600–900 °C		20–900 °C	130–600 °C	20–130 °C	600–900 °C		20–900 °C
Mass loss (%)	Structural H_2O	Moisture	CO_2	∑	Structural H_2O	Moisture	CO_2	∑	Structural H_2O	Moisture	CO_2	CO_2 and/or NaCl	∑	Structural H_2O	Moisture	CO_2	CO_2 and/or NaCl	∑	Structural H_2O	Moisture	CO_2	CO_2 and/or NaCl	∑
10/0	8.42	5.42	1.18	15.02	12.01	4.70	1.48	18.19															
10/1	8.33	4.20	2.19	14.72	12.43	5.83	1.71	19.97	12.87	5.70	3.18	–	21.75	12.70	5.99	2.31	–	21.00	14.00	4.40	3.80		22.20
10/2	8.00	4.18	1.70	13.88	11.62	4.50	3.11	19.23	12.36	6.45	2.84	–	21.65	13.07	6.26	3.10	–	22.43	13.52	5.60	4.10		23.22
10/3	8.22	6.46	2.15	16.83	11.27	8.43	2.56	22.26	11.83	7.65	3.01	–	22.49	12.06	8.65	2.81	–	23.52	13.00	7.90	3.30		24.20
10/4	8.07	7.81	2.04	17.92	10.61	9.93	2.69	23.23	11.24	10.28	3.50	–	25.02	13.59	10.53	2.36	–	26.48	13.99	9.91	3.40		27.30
10/5	7.82	8.48	1.93	18.23	9.22	13.28	4.10	26.60	12.32	12.73	2.36	–	27.42	13.89	12.09	2.84	–	28.82	13.80	12.30	3.90		30.00
10/1[a]	9.09	5.57	1.55	16.21	12.39	4.07	2.70	19.16	13.79	6.36	–	3.16	23.31	13.68	5.77	–	2.35	21.80	13.67	7.41		2.96	24.00
10/2[a]	9.39	4.28	1.97	15.64	12.83	5.73	2.40	20.96	13.03	4.93	–	2.40	20.36	12.86	5.98	–	2.16	20.90	12.43	5.36		3.02	20.80
10/3[a]	9.11	3.96	1.69	14.76	12.03	7.95	1.85	21.83	11.83	7.75	–	2.54	22.12	12.45	7.51	–	2.35	22.31	12.91	7.04		3.22	23.17
10/4[a]	9.15	7.03	1.73	17.91	10.65	12.18	2.93	25.76	11.19	9.97	–	4.07	25.23	13.02	11.30	–	4.19	28.51	13.53	8.04		4.45	26.02
10/5[a]	7.82	9.24	1.83	18.89	10.47	14.09	1.51	26.07	12.17	12.05	–	4.10	28.32	12.43	14.55	–	3.84	30.73	12.93	11.50		4.01	28.44
10/3[b]	12.44	4.92	2.91	20.27	13.22	6.44	2.19	21.85	13.33	6.99	2.62	–	22.94	13.36	6.55	2.82	–	22.73	13.43	5.92	3.52		22.87
10/3[c]	12.28	4.92	2.29	19.49	12.81	5.55	1.90	20.26	13.46	6.58	–	2.63	22.67	13.17	6.30	–	2.90	22.37	13.52	6.08		2.87	22.47

No symbol: 100% r.h.
[a] 100% r.h. + salt treatment.
[b] Steam-curing + 100% r.h.
[c] Steam-curing + salt treatment.

2.3.1. Hydration of C_4AF in water

If water reacts with C_4AF, similar phases are formed as in the case of C_3A hydration: hexagonal hydrates, which are later transformed into the stable phase, cubic hydrogarnet, $C_3/AF/H_6$. Three peaks are seen in the DTG curve of the no-gypsum sample, hydrated for 24 h: at 100°C, 170°C and 280°C, corresponding to moisture, hexagonal hydrates and hydrogarnet, respectively. This latter loses the remaining 1 mol of crystal water at 450°C (Fig. 1).

A "shoulder," at approximately 250°C, indicates the presence of hydrated iron oxide or alumina. The metal ion of these hydrated phases is not clear (even Mössbauer spectrometry did not give decisive results); some researchers [11] find the presence of $Fe(OH)_3$, while others [12,13] that of $Al(OH)_3$ more probable. The hexagonal hydrates → cubic hydrates transformation is slower in the case of C_4AF than in the case of C_3A.

Care must be taken when studying the hydration of C_4AF, as several factors may influence this reaction, e.g., even the mass of the reactants. Hydration is strongly exothermal, and the rate of hydration is temperature-dependent to a high extent, thus a higher mass of the solid may cause a local increase of temperature.

After 28 days of hydration, DTG curves are qualitatively similar, but intensities changed. The process of hydration is seen by the increased water loss, corresponding to the hydrogarnet phase (from 8.42% to 12.01%). The peak is uniform, without subpeaks, showing that a solid solution of C_3AH_6 and C_3FH_6 is formed.

2.3.2. Hydration of C_4AF+gypsum mixtures

The following phases can be detected in gypsum-containing samples besides the raw materials (C_4AF, gypsum): hexagonal hydrates ($C_2/AF/H_8$ or $C_4/AF/H_{13}$), cubic hydrate

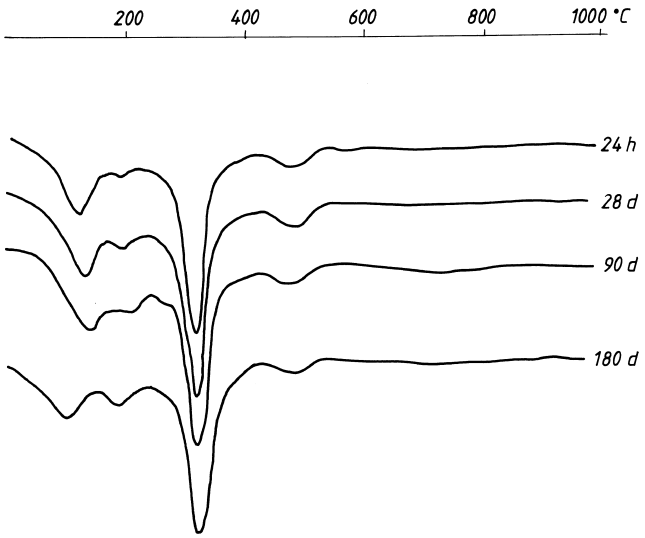

Fig. 1. DTG curves of hydrated C_4AF (Sample 10/0), after 1, 28, 90 and 180 days of curing.

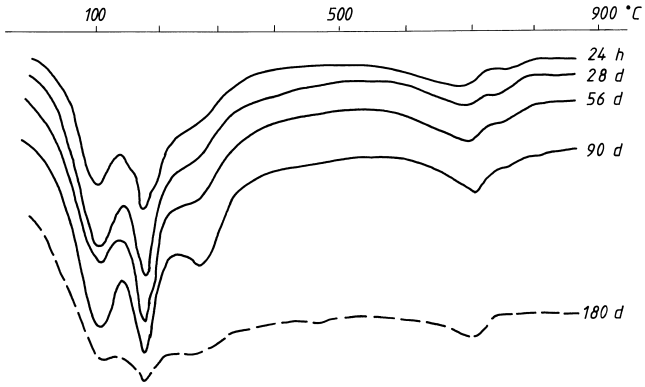

Fig. 2. DTG curves of hydrated C_4AF/gypsum (Sample 10/1), after 1, 28, 56, 90 and 180 days of curing.

($C_3/AF/_6$), ettringite (calcium-trisulfo-aluminate, $C_4/AF/\hat{S}_3H_{32}$), monosulfate (calcium-monosulfo-aluminate, $C_4/AF/\hat{S}H_{12}$), iron and/or aluminum hydroxide, as well as carbonates. Sample DTG curves are shown in Fig. 2.

In sample C_4AF, with gypsum in 10/1 mass ratio, after 24 h of hydration the DTG curve shows two intensive peaks, at approximately 100°C and 174°C. The former one can be attributed to the loss of moisture, but a part of ettringite crystal water is lost at the same temperature; this loss begins at approximately 50°C, but continues later, with a maximum rate at 140°C; while the one at 174°C shows the presence of $C_4/AF/H_{13}$, but with two "shoulders" at 140°C and 190°C; these are characteristic to the presence of ettringite and monosulfate, respectively. The peak at 700°C corresponds to the decarbonisation of calcium carbonate, formed by airborne CO_2. An upward bend of the DTG curve between 230°C and 400°C means weight loss, but cannot be assigned to one phase, as $C_4/AF/H_{13}$, hydrogarnet, ettringite and monosulfate lose water in this interval. After 28 days, the most intensive peak of the DTG curve can be seen at 180°C, but without the "shoulders," indicating that the ettringite → monosulfate transformation is almost finished by this time. After 56 days, only a slight change can be seen in the interval of 230–400°C: the one at 230°C can be attributed to alumina or iron hydroxide (or both), while the one at 280°C is due to the hydrogarnet phase, as the same one, but with an increased intensity is visible in the sample hydrated for 90 days, jointly with the 450°C peak. The most marked difference is the increase of the intensity of the 280°C peak. No essential quantitative changes can be seen in the 180-day-old sample, if contrasted to the 90-day-old one.

Results show that main hydration products of the 10/1 mixture of C_4AF and gypsum are: $C_3/AF/H_6$, $C_4/AF/H_{13}$, $C_3/AF/C\hat{S}H_{12}$ and hydrated alumina or iron oxide, or both.

Sample series 10/2 mixture of C_4AF and gypsum contains after 24 h of hydration ettringite, $C_4/AF/H_{13}$ and monosulfate, by DTG peaks at 140°C, 160°C and 185°C, as well as hydrogarnet, $C_3/AF/H_6$, by DTG peak 270°C. The 185°C peak is very intensive, still it does not merge with the $C_4/AF/H_{13}$ peak, 20–25°C lower, showing that there exists

a miscibility gap between these two complexes. No ettringite is found in older samples; AFm products are increasing. Moisture (100°C) and calcium carbonate (700°C) are present in all samples.

Sample series 10/3 mixture of C_4AF and gypsum contains after 24 h of hydration gypsum, ettringite, $C_4/AF/H_{13}$ and monosulfate, by DTG peaks at 140°C, 155°C and 175°C; hydrogarnet (270°C) content is much lower than in the 10/1 or 10/2 series at the same age. In older ages, $C_4/AF/H_{13}$, and monosulfate as well as hydrogarnet peaks, become more intensive; a small amount of ettringite (shoulder at 140°C) persists in the 28-day sample, but is absent later. Monosulfate peaks are more intensive than those of $C_4/AF/H_{13}$ at all ages. Main hydration products of series 10/3 are $C_3/AF/H_6$, $C_4/AF/H_{13}$ and $C_4/AF/\hat{S}H_{12}$.

In series 10/4 an intensive DTG peak can be seen after 24 h, between 20°C and 137°C, showing the presence of gypsum (double minima at 120°C and 135°C). All other products of hydration give shoulders rather than peaks. After 28 days, the 164°C peak ($C_4/AF/H_{13}$) is more intensive than that of the 182°C one (monosulfate), while in case of the older samples this order of intensity is inverted. The process of hydration can be seen by the increase of structural water content by 1–2%.

DTG curves of series 10/5 are qualitatively similar to the former one. Low-temperature (<120°C) peaks are very intensive because of the presence of unreacted gypsum. Several references exist [1,3,14,15], which claim that monosulfate is formed only after the exhaustion of gypsum by ettringite formation. In the case of high gypsum content (with the exception of the 24 h age), the $C_4/AF/H_{13}$ peak (170°C) is always more intensive than that of the monosulfate peak (190°C). Gypsum is present even after 180 days of 100% r.h. exposure.

2.3.3. Chloride binding capacity of C_4AF after NaCl exposure

It is a well established fact, that C_4AF binds chlorides, similarly to C_3A, by the formation of Friedel's salt $C_3A{\cdot}CaCl_2{\cdot}H_{10}$, or its iron analogue $C_3F{\cdot}CaCl_2{\cdot}H_{10}$, if chlorides are dissolved in the mixing water; hardly any data exist on hydrated C_3A or C_4AF exposed to chloride-containing water [5]. The question gets still more complicated in the case of hardened cement paste, and especially in the case of concrete, where other clinker minerals, admixtures, additives, aggregates all influence the nature of the hydration product. To clear these questions, a series of salt-treated samples was prepared: C_4AF–gypsum mixtures 10/1, 10/2, 10/3, 10/4 and 10/5 were hydrated in water for 28 days, and the hardened samples exposed 10% NaCl solution for 1 day, followed by 1 day of drying. This process was done from the 28th to the 56th day. After this time, the samples were kept in a 100% r.h. cabinet, as described in Section 2.1.

The most striking difference, as contrasted to non-salt-treated samples is the presence a flat, but well recognizable peak at approximately 310°C, which can be attributed to Friedel's salt, its iron analogue $C_3F{\cdot}CaCl_2{\cdot}10H_2O$ or their solid solution. About 40% of the water content of this phase is lost at 120–130°C. Other indications show that the chloro-aluminate ferrite AFm phase may form solid solutions with other sulfate-containing AFm phases or with $C_4/AF/H_{13}$.

Another interesting feature of the salt-treated samples is that the two high-temperature peaks, caused by decarbonisation (690°C and 770°C) are not present; on the other hand, a new peak, well distinguishable from former ones appears at 710°C. The disappearance of the CO_2 peaks is probably that the carbonate ion is incorporated into the AFm phases as hemi-, or monocarbo-aluminate; the new peak is due to the sublimation of NaCl from the surface of the sample. An interesting consequence of carbo-aluminate formation is the formation of secondary ettringite, as observed in Refs. [16,17]. They conclude that at high pH values (>12), the monosulfate is unstable in the presence of CO_2, and the sulfate can be replaced by the carbonate group, causing the formation of $C_3A{\cdot}CaCO_3{\cdot}H_{11}$; this increases the sulfate ion concentration of the solution and thus helps ettringite formation.

When comparing the DTG curves of salt-treated and non-salt-treated samples, at identical gypsum levels, no striking differences can be seen in younger (1- and 28-day) samples; in older samples, on the other hand, a new peak of 310°C appears, near the 260–270°C one. This is caused by Friedel's salt, or its iron-containing analogue. Another interesting feature, mentioned previously is that one peak appears (at 710°C), replacing the double peak of carbonates. The peak caused by AFm phases at approximately 180°C shows a single peak in salt-treated, rather than the double one (170°C and 190°C) in non-salt-treated samples (Fig. 3).

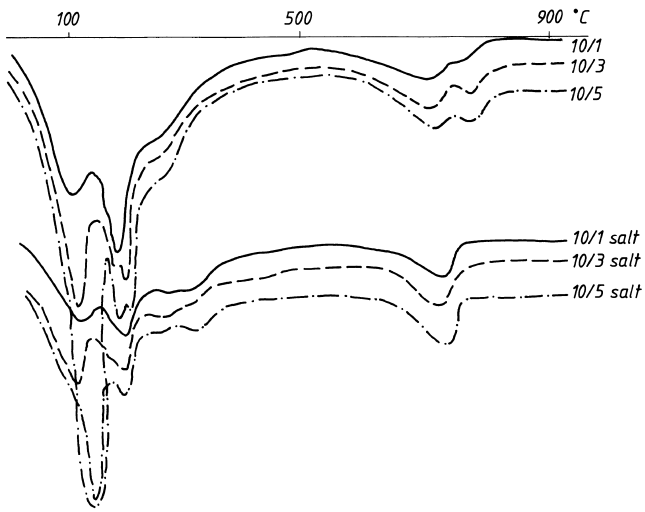

Fig. 3. Comparison of DTG curves of hydrated, and hydrated and salt-treated C_4AF/gypsum (Samples 10/1, 10/3 and 10/5), after 56 days of curing.

A next series was investigated to disclose the effect of steam-cured samples, both non-salt-treated and salt-treated ones. In this series, only the 10/3 C_4AF/gypsum sample was investigated. The main difference: AFm phases give a single peak at ~190°C. In the case of steam-cured samples, the two endproducts of hydration, i.e., $C_3/AF/H_6$ and monosulfate, are present even after 24 h. It looks like in the presence of gypsum the first step of hydration is the formation of ettringite; but steam-curing causes a rapid transformation of $C_4/AF/H_{13}$ to $C_3/AF/H_6$; as a gross effect, monosulfate and $C_3/AF/H_6$ are formed practically simultaneously.

It is a difficult task to calculate phase percentages using thermal analysis; the TGA curve, even with the aid of DTG, does not give exact information, not even when DTG peaks are well separated, as not only starting compounds react, but also newly formed ones, with themselves or with original ones. In our study, the Friedel's salt phase was approximately calculated by measuring the mass increase between 290°C and 330°C of salt-treated samples, compared to similar, but non-salt-treated ones (Table 3).

2.3.4. Conclusions of thermal testing

(1) The presence of calcium-aluminate/ferrite-chlorohydrate AFm phase, $C_3/AF/\cdot CaCl_2\cdot H_{10}$ was established, by its DTG peak between 290° and 315°C, in all salt-treated specimens, independently of the gypsum content. Fig. 3 compares non-salt-treated and salt-treated DTG curves of 10/1, 10/3 and 10/5 samples, age 56 days. Main differences in salt-treated samples:

- Appearance of the $C_3/AF/\cdot CaCl_2\cdot H_{10}$ peak at ~310°C.
- Broadening of the AFm peak (from 150–210°C to 130–210°C).
- Disappearance of the two carbonate peaks (670°C and 740°C); a single peak appears instead, at ~710°C, due to NaCl sublimation.

It should be mentioned, however, that in the case of non-salt-treated samples, the monosulfate peak (190°C) is more intensive, than that of the $C_4/AF/H_{13}$ (170°C) in the 10/3 mixture, while the intensity order is inverted in the 10/5 mixture. This shows that the metastable calcium-aluminate-ferrite-hydrate is more easily transformed into Friedel's salt (or its iron analogue) than the monosulfate phase.

Table 3
Quantity of $C_3/AF/\cdot CaCl_2\cdot H_{10}$ (%) in salt-treated C_4AF

C_4AF/gypsum	After 56 days	After 90 days	After 180 days	Average
10/1	–	–	–	–
10/2	7.7	7.7	–	7.7
10/3	–	–	15.3	15.3
10/4	–	–	–	–
10/5	–	22.9	23.0	23.0
10/3, steam-cured	–	9.6	9.6	9.6

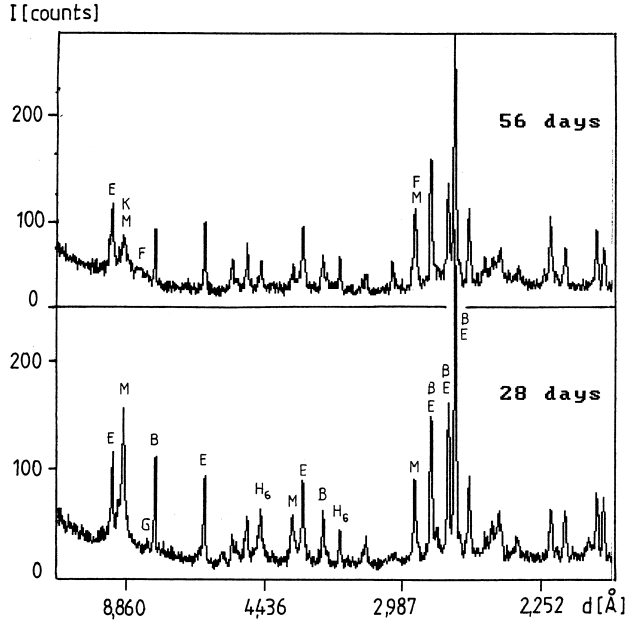

Fig. 4. XRD patterns of steam-cured C_4AF/gypsum (Sample 10/3), age 28 days and that of steam-cured and salt-treated C_4AF/gypsum (Sample 10/3), age 56 days. Symbols in all XRD patterns: B = aluminoferrite, E = ettringite, F = Friedel's salt, G = gypsum, M = monosulfate, $H_6 = C_3/AF/H_6$, K = Kuzel's salt.

This is why the most intensive 310°C peak appears at the 10/5 sample.

(2) It cannot be established if Friedel's salt, or its iron analogue or their solid solution are present, as they have identical crystal structures and thus thermal peaks (and also X-ray patterns) are similar.

(3) All AFm phases ($C_4/AF/H_{13}$, monosulfate, iron monosulfate, Friedel's salt, iron Friedel's salt or even $C_3/AF/CaCO_3\cdot H_{11}$) may form solid solutions, but usually a miscibility gap exists between them. This is why the DTG peak at ~160–200°C is sometimes single, and sometimes divided to partial minima.

2.3.5. Additional results of C_4AF hydration by XRD

XRD was used as an additional method to characterize most of the samples; although thermal tests enable a quantitative characterization, but in multicomponent systems, if several compounds give a DTA/DTG peak in the same temperature interval, phase identification is not always possible. XRD can qualitatively help in such cases, using a computer comparison of known XRD patterns [18] with our own patterns. It should be mentioned that all results of the former paragraphs had been corroborated by XRD results.

Only some sample XRD patterns are shown in this paper. Steam-cured sample 10/3 after 28 days shows intensive peaks of monosulfate ($C_4/AF/\hat{S}H_{12}$), ettringite ($C_6/AF/\hat{S}_3H_{31}$) and those of unhydrated C_4AF. Low-intensity peaks indicate the presence of small quantities of $C_3/AF/H_6$ and gypsum (Fig. 4). In the same material, after NaCl curing, the pattern shows the presence of the chloride-containing

Table 4
C_6A_2F mass losses by TGA (initial sample mass = 100)

Age	24 h				28 days				56 days				90 days				180 days			
Temperature interval	130–600 °C	20–130 °C	600–900 °C	20–900 °C	130–600 °C	20–130 °C	600–900 °C	20–900 °C	130–600 °C	20–130 °C	600–900 °C	20–900 °C	130–600 °C	20–130 °C	600–900 °C	20–900 °C	130–600 °C	20–130 °C	600–900 °C	20–900 °C
Mass loss (%)	Structural H_2O	Moisture	CO_2	$\sum$	Structural H_2O	Moisture	CO_2	$\sum$	Structural H_2O	Moisture	CO_2 and/or NaCl	$\sum$	Structural H_2O	Moisture	CO_2 and/or NaCl	$\sum$	Structural H_2O	Moisture	CO_2 and/or NaCl	$\sum$
10/0	12.4	7.8	0.7	20.9	17.0	3.8	1.2	22.0	20.1	7.1	– 2.7	29.9	21.2	3.2	– 3.4	27.8				
10/1	10.6	3.9	1.9	16.4	14.8	5.7	1.9	22.4	14.5	6.9	1.7 –	23.1	14.6	7.5	1.7 –	23.8	15.4	8.3	3.1 –	26.8
10/2	11.7	6.5	2.2	20.4	15.2	5.6	2.7	23.5	15.2	7.3	2.6 –	25.1	18.7	5.2	2.1 –	14.0	20.6	8.6	2.1 –	31.3
10/3	11.1	5.8	2.4	19.3	15.2	6.9	2.5	24.7	15.9	6.5	2.6 –	25.0	16.8	4.3	2.9 –	24.0	16.5	7.3	3.4 –	27.2
10/4	10.9	6.7	2.2	19.8	14.2	7.1	2.6	23.9	15.6	8.9	2.9 –	27.4	15.5	7.3	2.6 –	25.4	16.3	7.2	2.5 –	26.0
10/5	9.5	9.8	1.9	21.2	13.2	10.3	2.8	26.3	13.6	11.2	2.7 –	27.5	14.0	9.5	2.6 –	26.1				
10/1[a]	9.4	6.1	1.7	17.2	12.9	8.8	2.3	24.0	13.8	5.6	– 3.1	22.5	15.1	5.8	– 3.1	24.0				
10/2[a]	9.1	5.8	1.7	16.6	14.0	7.5	2.1	23.6	15.1	6.3	– 2.9	24.3	14.6	6.3	– 2.1	23.0	19.5	9.8	– 2.6	31.9
10/3[a]	7.8	7.1	2.1	17.0	13.2	6.9	2.1	22.2	14.1	6.9	– 3.4	24.4	13.6	5.7	– 3.1	22.4				
10/4[a]	7.4	8.9	1.9	18.2	12.5	9.5	2.0	24.0	13.2	8.5	– 4.1	25.8	12.8	8.7	– 2.9	24.4				
10/5[a]	7.6	12.5	2.0	22.1	12.3	12.4	2.4	27.1	14.0	14.6	– 4.2	32.8	14.0	10.9	– 3.8	28.7	16.4	21.2	– 4.7	42.4
10/3[b]	13.2	6.6	2.1	21.9	16.1	6.9	2.4	25.4	16.1	5.6	3.2 –	24.9	17.1	7.6	1.5 –	26.2				
10/3[c]	13.2	5.4	2.2	20.8	16.0	9.5	2.6	22.5	16.9	4.7	– 4.2	25.8	16.9	7.6	– 1.8	26.3				

No symbol: 100% r.h.
[a] 100% r.h. + salt treatment.
[b] Steam-curing + 100% r.h.
[c] Steam-curing + salt treatment.

Table 5
C_6AF_2 mass losses by TGA (initial samples mass = 100)

Age	24 h				28 days				56 days					90 days					180 days				
Temperature interval	130–600 °C	20–130 °C	600–900 °C	20–900 °C	130–600 °C	20–130 °C	600–900 °C	20–900 °C	130–600 °C	20–130 °C	600–900 °C		20–900 °C	130–600 °C	20–130 °C	600–900 °C	20–900 °C		130–600 °C	20–130 °C	600–900 °C	20–900 °C	
Mass loss (%)	Struct. H_2O	Moisture	CO_2	∑	Structural H_2O	Moisture	CO_2	∑	Structural H_2O	Moisture	CO_2	CO_2 and/or NaCl	∑	Structural H_2O	Moisture	CO_2 and/or NaCl		∑	Structural H_2O	Moisture	CO_2 and/or NaCl		∑
10/0	11.6	9.5	1.0	21.1	21.3?	10.4	1.8	34.5	17.7	8.7	3.3		29.8										
10/1	9.2	5.6	2.1	16.9	12.6	7.3	2.3	22.2	14.9	7.2	2.5	–	24.6	15.6	8.9	2.6		24.1	17.2	7.1	3.7	–	28.0
10/2	8.6	7.8	1.9	18.3	12.5	9.2	2.3	24.0	16.9	11.4	1.9	–	30.2	15.7	8.5	3.1		27.3	18.0	9.9	2.7	–	30.6
10/3	8.5	11.0	0.9	20.4	12.9	13.5	1.4	27.8						16.9	12.3	2.7		31.9	13.0	10.9	2.2	–	26.1
10/4	7.8	10.2	1.2	19.2	13.3	17.6	1.4	32.3	16.4	20.2	1.6	–	38.2	15.7	16.8	2.8		35.3	12.4	15.2	2.8	–	30.4
10/5	9.3	12.4	1.2	22.9	13.8	23.4	1.7	38.9	14.9	22.5	1.8	–	39.2	14.7	20.0	3.4		38.1	10.9	16.4	2.3	–	29.9
10/1[a]	9.0	5.1	2.0	16.1	13.3	4.9	2.2	20.4	14.6	7.7	–	2.4	24.7	12.3	5.9	–	3.5	21.7	15.4	8.0	–	3.1	26.5
10/2[a]	8.8	9.1	1.4	19.3	12.5	9.6	1.7	23.8	15.0	14.8	–	3.1	33.8						18.0	11.3	–	2.9	32.2
10/3[a]	8.5	10.2	1.0	19.7	13.2	13.9	1.4	28.5	17.0	13.8	–	4.1	34.9	15.4	17.9	–	4.0	37.3	19.3	13.7	–	2.9	35.9
10/4[a]	8.3	9.8	1.1	19.2	13.2	18.7	1.5	33.4	18.9	25.6	–	4.7	49.2	12.0	24.1	–	5.2	41.3	14.1	39.3	–	2.7	52.1
10/5[a]	9.0	11.2	1.1	21.3	13.9	21.9	1.6	37.4	11.8	18.4		3.3	33.5	12.3	25.4	–	4.4	42.1	13.9	37.0	–	4.6	55.5
10/3[b]	11.1	15.1	1.5	27.7	15.1	13.8	1.4	30.3	17.2	17.1	1.7	–	36.0	15.5	14.4	2.1	–	32.2	13.1	12.2	2.2	–	27.5
10/3[c]	11.2	15.3	1.2	27.7	15.8	11.6	2.4	29.8	16.0	16.8		2.1	34.9	16.4	15.5		3.1	35.0	19.7	21.1	–	3.7	44.5

No symbol: 100% r.h.
[a] 100% r.h. + salt treatment.
[b] Steam-curing + 100% r.h.
[c] Steam-curing + salt treatment.

AFm phase, $C_3/AF/\cdot CaCl_2\cdot H_{10}$ too, while gypsum is not present anymore.

Although XRD was used as an additional method only, still it can give interesting informations. On the DTG curve of steam-cured sample 10/3 and the same, but salt-treated one, age 56 days the AFm peaks are of similar intensity; still their XRD patterns are different: In the non-salt treated sample monosulfate reflections are intensive, while in the salt-treated, but otherwise similar sample, these peaks are faint. Reflections of Friedel's salt are also weak, but among the low-intensity peaks, between 7.8 and 9.6 Å lattice spacings, a new peak can be seen at 8.51 Å. This peak can be assigned to Kuzel's salt [17], $C_3/AF/\cdot 1/2CaSO_4\cdot 1/2CaCl_2\cdot H_{11}$. Solid solubility of Friedel's salt, Kuzel's salt and other AFm phases exists, but with certain gaps. Friedel's salt stabilizes the monosulfate phase by the formation of Kuzel's salt.

Unfortunately, neither thermal tests nor XRD can differentiate between C_3AH_6, C_3FH_6, and their solid solution $C_3/AF/H_6$, and similarly between $C_3A\cdot CaCl_2\cdot H_{10}$, $C_3F\cdot CaCl_2\cdot H_{10}$, and their solid solution $C_3/AF/\cdot CaCl_2\cdot H_{10}$. XRD, on the other hand, gives surplus information on the presence of ettringite: Small XRD peaks of ettringite are seen even if the DTG curve shows no peaks. In the 10/2 mixture, after 56 days of hydration, gypsum XRD peaks are still visible, jointly with strong monosulfate peaks. The theory, which claims that monosulfate occurs only after the total exhaustion of gypsum, is false.

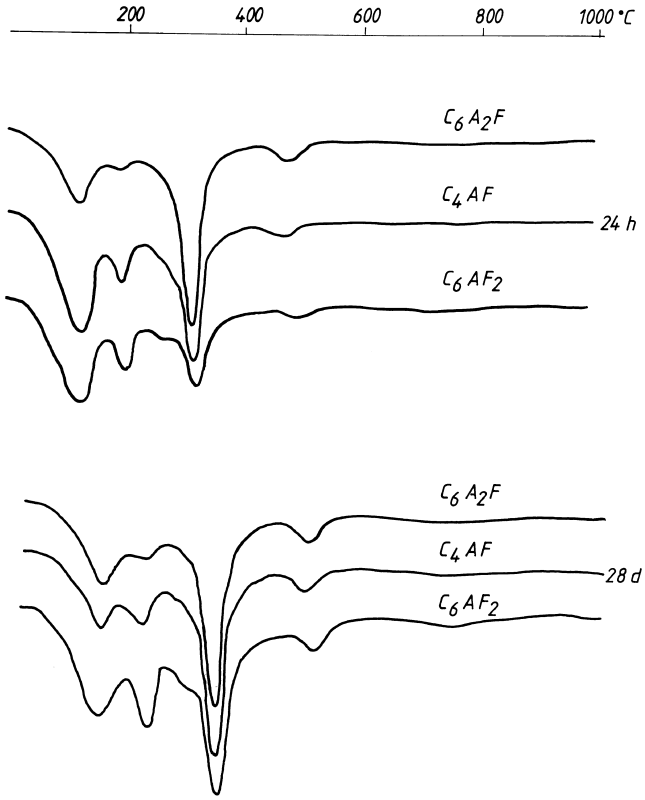

Fig. 5. DTG curves of C_6A_2F, C_4AF and C_6AF_2 samples after 24 h and 28 days of hydration.

2.4. Hydration of C_6A_2F and C_6AF_2

The hydration and chloride binding capacity of these two aluminoferrites are qualitatively similar, but differences exist in the rate of hydration and consequently, the amount of hydration products. Mass losses by TGA are given in Tables 4 and 5, for C_6A_2F and C_6AF_2, respectively. Besides, some sample DTG curves are presented.

2.5. Comparison of C_42F, C_6A2F and C_6AF_2 hydration and chloride binding capacity

Hydration products of the three aluminoferrites C_4AF, C_6A_2F and C_6AF_2 are similar: without gypsum, $C_3/AF/H_6$, $C_3/AF/H_{13}$, $Fe(OH)_3$ and/or $Al(OH)_3$ are formed, but the rate is different (Fig. 5). It is a well-known fact that the hydration of tricalcium aluminate is faster than that of brownmillerite. This rule is followed by the aluminoferrites, too: hydration rate increases in the order $C_6A_2F>C_4AF>C_6AF_2$. This can be illustrated, e.g., by the structural water content (weight loss between 130°C and 600°C, in percent) of the 10/3 steam-cured samples, at the age of 24 h: $C_6A_2F = 13.2$; $C_4AF = 12.4$; $C_6AF_2 = 11.1$.

It is clear that the rate of hydration decreases with increasing iron content. Above data show, that from that point C_4AF is somewhat closer to C_6A_2F than to C_6AF_2. The selection of steam-cured samples was not arbitrary; hydration rate depends strongly on temperature and a small change in room temperature may have a higher effect than the iron content of the aluminoferrite phases.

In the presence of gypsum, other phases (ettringite and/or monosulfate) are formed, too; hydration rate decreases almost proportionally by the percentage of gypsum. This rate-decreasing effect can be explained in a dual way: The higher concentration of sulfate ions hinders the transformation of hexagonal hydrates to the cubic $C_3/AF/H_6$ phase. Another cause, especially in the case of high gypsum additions is that a high sulfate content stabilizes ettringite and thus partly or fully prevents monosulfate formation. In the case of C_6A_2F/gypsum mixtures, the presence of $C_3/AF/H_6$ can be detected even after 24 h, irrespectively of the gypsum content, while in the case of C_4AF this phase can be observed after 24 h only in 10/1 and 10/2 mixtures; at higher gypsum additions (10/3, 10/4 and 10/5) at the age of 28, 90 and 180 days, respectively. In the case of C_6AF_2/gypsum mixtures, the presence of $C_3/AF/H_6$ can be detected after 28 days of curing in the 10/1 and 10/2 samples, and after 56 days of curing in the 10/3 sample. In the case of still higher gypsum content (mixtures 10/4 and 10/5), the hydrogarnet is not formed, even after 180 days.

All three aluminoferrites hydrate in a similar way; in the presence of gypsum the following phases can be detected: ettringite, monosulfate, hexagonal hydrates, hydrogarnet, iron and/or aluminum hydroxide. The chloride binding

ability is also similar: All three aluminoferrites bind ingressing Cl^- ions in the form of Friedel's salt, or its iron-containing analogue. As both $C_3A{\cdot}CaCl_2{\cdot}H_{10}$ and $C_3F{\cdot}CaCl_2{\cdot}H_{10}$ and their solid solution, $C_3/AF/{\cdot}CaCl_2{\cdot}H_{10}$ have similar structures, neither thermal curves, nor XRD patterns can differentiate between them. Chloride binding capacity of these phases can be seen in Fig. 6 where DTG curves of hydrated (28 days of age) and salt-treated (56 days of age) are shown for C_4AF, C_6A_2F and C_6AF_2 samples.

It is striking that in the case of C_6A_2F and C_6AF_2, the hydrogarnet peak (280°C) and Friedel's salt (or analogue) peak (310°C) are divided, or, more correctly two partial minima can be seen, while in the case of C_4AF only a broadening of the 280°C peak can be observed. This is true for hydrated and salt-treated samples, too, although a shift of the minimum towards higher temperatures is evident. Another interesting observation is the broadening of the DTG peak due to AFm, at 150°C.

The formation of $C_3/AF/{\cdot}CaCl_2{\cdot}H_{10}$ in function of gypsum content can be well seen in Fig. 7, which shows DTG curves of hydrated/salt-treated C_6AF_2, 10/1–10/5 mixtures. (This high-iron material gives the least quantity of hydrogarnet). This figure shows that the 310°C peak (due to $C_3/AF/{\cdot}CaCl_2{\cdot}H_{10}$) is the most intensive in the 10/3 mixture, while in case of the 10/4 and 10/5 samples no (or negligible) amount of $C_3/AF/{\cdot}1/2CaCl_2{\cdot}1/2CaSO_4.H_{11}$ are formed as the intensity of the AFm peak is lower as contrasted to the 10/1, 10/2 and 10/3 samples. In the C_6AF_2 + gypsum + water system, the OH-AFm phase has the least stability, thus the $OH^- \rightarrow Cl^-$ exchange has a high probability. X-ray evidence also shows that in 10% NaCl solution, the SO_4^{2-} group is substituted by Cl^-.

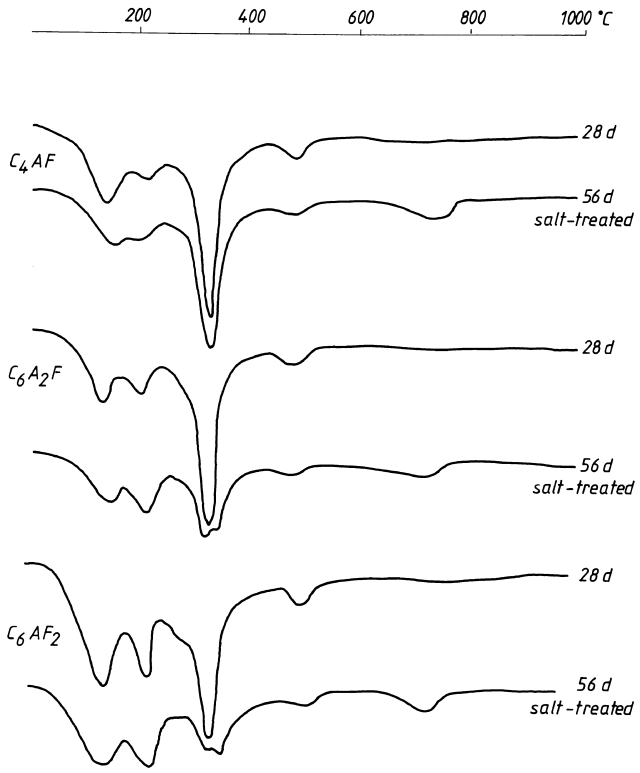

Fig. 6. DTG curves of hydrated (28 days) and hydrated, salt-treated (56 days) C_4AF, C_6A_2F and C_6AF_2 samples.

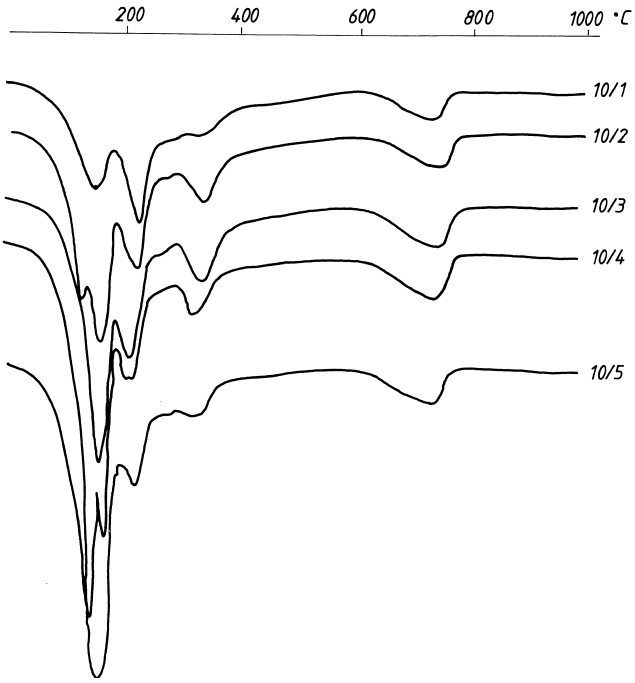

Fig. 7. DTG curves of hydrated, salt-treated (56 days) 10/1, 10/2, 10/3, 10/4 and 10/5 C_6AF_2 samples.

DTG curves of salt-treated, 10/3 C_4AF/gypsum and 10/3 C_6AF_2/gypsum samples are shown in Fig. 8. It looks like more chloride is bound by C_6AF_2 than by C_4AF as the 310°C peak (caused by Friedel's salt and/or its iron analogue) has a higher intensity in this case. On the C_4AF curve, on the other hand, the AFm peak (155°C) is broader, showing that Friedel's salt can be present as a solid solution (anionic Cl^- replaced partly or fully by OH^- or as Kuzel's salt, $C_3/AF/{\cdot}1/2CaCl_2{\cdot}1/2CaSO_4{\cdot}H_{11}$).

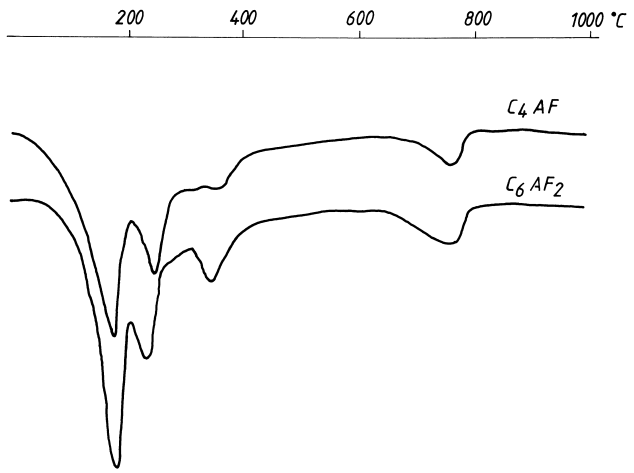

Fig. 8. DTG curves of hydrated, salt-treated (56 days) 10/3 C_4AF and C_6AF_2 samples.

Table 6
Quantity of $C_3/AF/\cdot CaCl_2\cdot H_{10}$ in salt-treated C_6AF_2 (initial sample mass = 100)

C_6AF_2/gypsum	After 56 days	After 90 days	After 180 days	Average
10/1	7.8	7.2	6.5	7.2
10/2	18.1	–	15.8	16.9
10/3	18.1	–	18.1	18.1
10/4	12.9	12.9	12.9	12.9
10/5	13.4	–	12.1	12.7
10/3, steam-cured	9.6	13.0	15.0	12.5

It has been tried to estimate the quantity of bound chloride (in the form of $C_3/AF/\cdot CaCl_2\cdot H_{10}$) in the case of C_6AF_2 and C_4AF (the former phase was selected as there high quantities of Friedel's salt, and low quantities of hydrogarnet are formed). The basis of this estimation: of the 10 mol of Friedel's salt crystal water 6 and 4 mol are lost at 310°C and 120°C (see Table 6).

In general, hydrated AFm phases show only one, regular DTG minimum, without being subdivided by partial minima, in the case of all three aluminoferrites, if the mixing ratio was 10/1. This shows that only a solid solution is formed. In the 10/2 mixture, as more monosulfate is formed, by the increased gypsum content, the formation of solid solutions is incomplete, and both $C_4/AF/H_{13}$ (170°C) and monosulfate (190°C) can be detected.

In salt-treated samples, AFm phases give always a regular, not subdivided DTG peak. This is a consequence of both aluminum- and iron-containing Friedel's salt, which may take part in solid solution formation. Another possibility of solid solubility includes OH^--containing AFm phases. Monosulfate is stabilized in the form of Kuzel's salt, $C_3/AF/\cdot 1/2CaCl_2\cdot 1/2CaSO_4\cdot H_{11}$) and this can form solid solutions with other AFm phases. The least stable of these phases is OH^--AFm, but this can be stabilized by anion substitution.

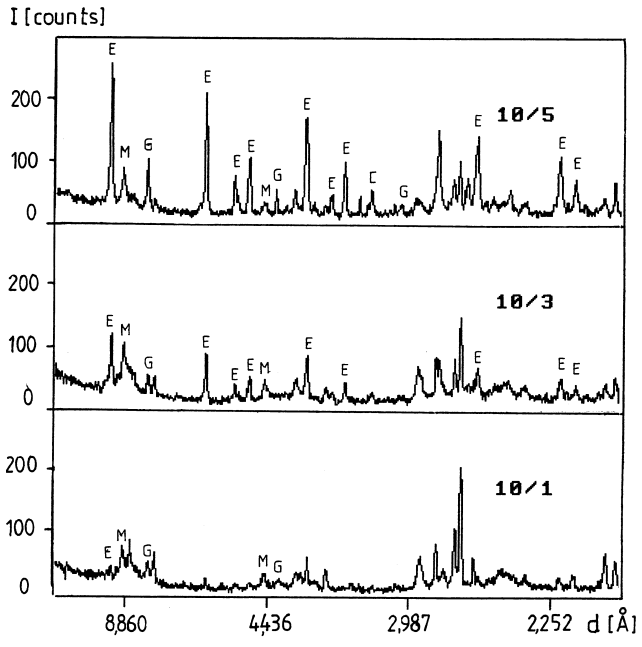

Fig. 9. XRD patterns of C_6AF_2, 10/1, 10/3 and 10/5, hydrated for 28 days.

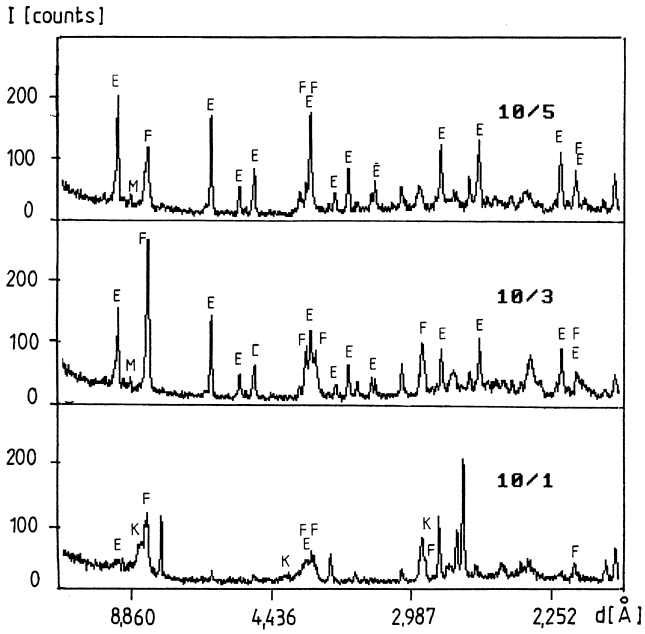

Fig. 10. XRD patterns of C_6AF_2, 10/1, 10/3 and 10/5, salt-treated (56 days).

Two sample XRD patterns are shown, too: in Fig. 9 the hydration of C_6AF_2 can be followed, in the presence of gypsum, age 28 days, while in Fig. 10 the same aluminoferrite, salt-treated, after 56 days, is shown.

The role of gypsum from the point of Cl binding is manifold: it improves chloride binding by hindering the $C_4/AF/H_x \rightarrow C_3/AF/H_6$ transformation; another function of gypsum is the hindering of the ettringite → monosulfate transformation and consequently, decreases Kuzel's salt formation. This salt is a "hybride" of Friedel's salt and monosulfate.

3. Summary and conclusions

(1) Hydration products of aluminoferrites (C_4AF, C_6A_2F, C_6AF_2) are similar to those of C_3A; only alumina is partly or fully replaced by iron oxide. The transformation rate of metastable iron-containing calcium-aluminate-ferrite-hydrates ($C_4/AF/H_{13}$, $C_2/AF/H_8$), to the stable hydrogarnet phase, however, is slower, than in the case of iron-free compounds (although $C_3/AF/H_6$ is present even after 1 day of hydration). C_3AH_6, C_3FH_6 or their solid solution $C_3/AF/H_6$ cannot be distinguished by the methods (thermal analysis, XRD) used in this study.

(2) Hydration products of aluminoferrite + gypsum mixtures are, besides those mentioned under (1), are monosulfate ($C_3/AF/\cdot CaSO_4\cdot H_{12}$) and ettringite ($C_3/AF/\cdot 3CaSO_4\cdot H_{31}$). Monosulfate was found, a contrary to Ref.

[1], prior to the total exhaustion of gypsum. Ettringite, in some cases, was not detectable by thermal tests due to its low quantity but was seen in low-intensity peaks on XRD patterns. Metastable hexagonal hydrates, of general formula $[Ca_2/Al,Fe/(OH)_6]OH{\cdot}xH_2O$ were detected by thermal tests in each of the non-steam-cured samples.

(3) In all salt-treated aluminoferrite/gypsum mixtures, the AFm phase, Friedel's salt ($C_3/AF/{\cdot}CaCl_2{\cdot}H_{10}$) was detected, by thermal as well as XRD tests, independently of the gypsum quantity.

(4) Monosulfate is transformed into Friedel's salt especially in steam-cured and salt-cured specimens.

(5) The AFm phases $C_4/AF/H_{13}$, $C_4/AF/\hat{S}H_{12}$, $C_3/AF/{\cdot}CaCl_2.H_{10}$, $C_4/AF/\hat{C}H_{12}$ may form solid solutions; this series is not continuous. This explains the fact that the DTG peak of the AFm phases is sometimes single, and sometimes divided by a transient maximum. After salt treatment, however, AFm phases show a single minimum on the DTG curve.

(6). Less Cl^- was bound in steam-cured ferrite phases than in similar, but non-steam-cured samples.

(7) The iron content of aluminoferrites does not qualitatively influence hydration reactions; but the hydration rate is different. Rate increases in the order of $C_6A_2F>C_4AF>C_6AF_2$.

(8) The stability of AFm phases is very important from the point of concrete performance.

Acknowledgments

This research was supported by the Hungarian National Scientific Research Foundation (OTKA), Grant No. T019414. Authors are grateful for funding and continuous support of OTKA. Ferrite material (C_4AF, C_6A_2F, C_6AF_2) was provided by CEMKUT (Budapest) and personally by Dr. M. Révay. XRD investigations were done at the Department of Mineralogy, Technical University of Budapest. Authors are indebted to Mrs. K. Kopecsko-Kocsányi for XRD investigations, and Mrs. E. Felszeghy for DTG tests.

References

[1] M. Collepardi, S. Monosi, G. Moriconi, M. Corradi, Tetracalcium-aluminoferrite hydration in the presence of lime and gypsum, Cem. Concr. Res. 9 (4) (1979) 431–437.
[2] A. Emanuelson, S. Hansen, Distribution of iron among ferrite hydrates, Cem. Concr. Res. 27 (8) (1997) 1167–1177.
[3] A.K. Suryavanshi, J.D. Scantlebury, S.B. Lyon, The binding of chloride ions by sulphate resistant portland cement, Cem. Concr. Res. 25 (3) (1995) 581–592.
[4] U.A. Birnin-Yauri, F.P. Glasser, Friedel's salt, $Ca_2Al(OH)_6(Cl,OH){\cdot}2H_2O$: Its solid solutions and their role in chloride binding, Cem. Concr. Res. 28 (12) (1998) 1713–1724.
[5] A.K. Suryavanshi, R. Narayan Swamy, Stability of Friedel's salt in carbonated concrete structural elements, Cem. Concr. Res. 26 (5) (1996) 729–742.
[6] R. Rasheeduzzafar, S. Entesham Hussain, S.S. Al-Sadoom, Effect of cement composition on chloride bonding and corrosion of reinforcing steel in concrete, Cem. Concr. Res. 21 (5) (1991) 777–794.
[7] S. Entesham Hussain, S. Rasheeduzzafar, A.S. Al-Gahtani, Influence of sulfates on chloride binding in cements, Cem. Concr. Res. 24 (1) (1994) 8–24.
[8] Y. Xu, Influence of sulfates on chloride binding and pore solution chemistry, Cem. Concr. Res. 27 (12) (1997) 1841–1850.
[9] A.A. Tabikh, R.J. Weht, An XRD analysis of portland cement, Cem. Concr. Res. 1 (3) (1971) 317–328.
[10] F.D. Tamás, K. Kovács, A generalization and computer solution of the Bogue calculation, Cem. Technol. 5 (4) (1974) 393–401.
[11] J.M. Fortune, J.M.D. Coey, Hydration products of calcium aluminoferrite, Cem. Concr. Res. 13 (5) (1983) 696–702.
[12] F.D. Tamás, A. Vértes, Brownmillerite hydration by Mössbauer spectrometry, Hung. J. Ind. Chem. 3 (3) (1975) 337–385.
[13] K.S. Harchand, R. Kumar, K. Chandra, Vishwamittar, Mössbauer and X-ray investigations on some portland cements, Cem. Concr. Res. 14 (2) (1984) 170–176.
[14] Gy. Balázs, J. Csizmadia, K. Kovács, Chloride ion binding ability of calcium-aluminate, -ferrite and -silicate phases, Period. Polytech. 41 (2) (1997) 147–168.
[15] I. Jawed, S. Goto, R. Kondo, Hydration of tetracalcium aluminoferrite in the presence of lime and sulfates, Cem. Concr. Res. 6 (3) (1976) 441–454.
[16] F.P. Glasser, A. Kindness, S.A. Stronach, Stability and solubility relations in Afm phases: Part I. Chloride, sulfate and hydroxide, Cem. Concr. Res. 29 (6) (1999) 861–866.
[17] H.-J. Kuzel, H. Pöllmann, Hydration of C_3A in the presence of $Ca(OH)_2$, $CaSO_4{\cdot}2H_2O$ and $CaCO_3$, Cem. Concr. Res. 21 (1991) 885–896.
[18] H.F.W. Taylor, Cement Chemistry, Academic Press, New York, 1990.